Physica A 392 (2013) 6330–6340

Contents lists available at ScienceDirect

Physica A

journal homepage: www.elsevier.com/locate/physa

Site–bond percolation on triangular lattices: Monte Carlo simulation and analytical approach

M.I. González [a,b], P. Centres [b], W. Lebrecht [a], A.J. Ramirez-Pastor [b], F. Nieto [b,*]

[a] Departamento de Física, Universidad de La Frontera, Casilla 54-D, Temuco, Chile

[b] Departamento de Física, INFAP, Universidad Nacional de San Luis, CONICET, Chacabuco 917, D5700BWS San Luis, Argentina

HIGHLIGHTS

- Phase diagram of the site–bond percolation on triangular lattice is studied.
- Two distinct schemes (denoted as $S \cap B$ and $S \cup B$) for site–bond percolation are used.
- The phase diagram is obtained via Finite-size scaling analysis.
- A theoretical approach based on counting configurations on finite cells is applied.
- The phase diagram is determined by Monte Carlo and the theoretical approach.

ARTICLE INFO

Article history:
Received 22 October 2012
Received in revised form 22 August 2013
Available online 8 September 2013

Keywords:
Percolation
Monte Carlo simulation
Phase transitions

ABSTRACT

A generalization of the pure site and pure bond percolation problems called site–bond percolation on a triangular lattice is studied. Motivated by considerations of cluster connectivity, two distinct schemes (denoted as $S \cap B$ and $S \cup B$) for site–bond percolation are used. In $S \cap B$ ($S \cup B$), two points are said to be connected if a sequence of occupied sites *and* (*or*) bonds joins them. By using finite-size scaling theory, data from $S \cap B$ and $S \cup B$ are analyzed in order to determine (*i*) the phase boundary between the percolating and non-percolating regions and (*ii*) the numerical values of the critical exponents of the phase transition occurring in the system. A theoretical approach, based on exact calculations of configurations on finite triangular cells, is applied to study the site–bond percolation on triangular lattices. The percolation processes have been monitored by following the percolation function, defined as the ratio between the number of percolating configurations and the total number of available configurations for a given cell size and concentration of occupied elements. A comparison of the results obtained by these two methods has been performed and discussed.

1. Introduction

The percolation problem has been a focal point of statistical mechanics research for several decades [1–6]. One reason for this current interest is that it is becoming clear that generalizations of the pure percolation problem are likely to have extensive applications in the description of various phenomena in nature. Although it is a purely geometric phenomenon, the phase transition involved in the process can be described in terms of the usual second order phase transition. This mapping to critical phenomena made percolation a full part of the theoretical framework of collective phenomena and statistical physics.

* Correspondence to: Departamento de Física, Universidad Nacional de San Luis, CONICET, Chacabuco 917, 5700 San Luis, Argentina. Tel.: +54 266 4436151; fax: +54 266 4430224.
E-mail addresses: fnieto@unsl.edu.ar, cachonieto@gmail.com (F. Nieto).

0378-4371/$ – see front matter
http://dx.doi.org/10.1016/j.physa.2013.09.001

The central idea of the pure percolation theory is based on finding the minimum concentration of elements (sites or bonds) for which a cluster extends from one side to the opposite one of the system. This particular value of the concentration rate is named *critical concentration* or *percolation threshold* and determines a phase transition in the system. Thus, in the random percolation model, a single site (or a bond connecting two sites) is occupied with probability p. For the precise value of p_c, the percolation threshold of sites (bonds), at least one spanning cluster connects the borders of the system (indeed, there exist a finite probability of finding $n\,(>1)$ spanning clusters [7–10]). In that case, a continuous phase transition appears at p_c which is characterized by well defined critical exponents.

More general percolation problems can be formulated by assuming that both sites and bonds are randomly and independently occupied with occupancy fractions p_s and p_b, respectively. We may then define *site-and-bond* ($S \cap B$) and *site-or-bond* ($S \cup B$) percolation: in $S \cap B$, a cluster is considered to be a set of occupied bonds and sites in which the bonds are joined by occupied sites, and the sites are joined by occupied bonds. $S \cap B$ represents the well-known site–bond percolation, which has many applications in different fields. For instance, it was used to describe the sol-to-gel transition (gelation) of polymers [11]. In this model, bonds represent chemical bonds, occupied sites represent monomers, and empty sites represent solvent molecules. Sites are correlated as in a lattice gas model of a binary mixture. In $S \cup B$, a bond or site contributes to cluster connectivity independently of the occupation of its endpoints.

The phase diagram of the site–bond system in the $p_s - p_b$ parameter space has been widely studied, in particular for a square lattice. Thus, the model was mentioned at first by Frisch and Hammersley [12]. Agrawal et al. [13] and Nakanishi and Reynolds [14] showed, by using a series method and position-space renormalization group, respectively, that the critical exponents of pure site percolation are also valid for site–bond percolation. Later, Yanuka and Englman [15] proposed an equation for the critical curve separating the sol-to-gel transition in the site–bond percolation model, for square, triangular, simple cubic and face centered cubic (fcc) lattices. More recently, Tarasevich and van der Marck [16] presented a very complete and systematic study, where site–bond percolation thresholds were calculated by means of numerical simulations in many lattices in two to five dimensions. The critical curve corresponding to the $S \cap B$ problem, is a line which separates the percolating, in which a gel is formed, and the non percolating area, the sol phase. On the other hand, the percolating and the non-percolating region corresponding to the $S \cup B$ problem are separated by a different critical curve. Standard site (bond) percolation is recovered as the $p_b = 1$ ($p_s = 1$) case of the $S \cap B$ problem, as well as $p_b = 0$ ($p_s = 0$) case of the $S \cup B$ problem. Note that p_s^c and p_b^c represent the percolation thresholds of standard site and bond percolation. The site–bond percolation phase diagram for different geometries has received considerably less attention [17–21]. In particular, the corresponding phase diagram for triangular geometry is poorly referenced in the literature.

In this context, the aim of the present paper is (a) to determine, via MC simulations and finite-size scaling theory, the phase diagram in the $p_s - p_b$ space for site and bond independently and randomly deposited on a triangular lattice; (b) to verify the universality class of the phase transition involved in the problem and (c) to give an approximative theoretical expression for the phase diagram in order to explain the general features of the curves based in essentially simple assumptions. The proposed system is the simplest model including the essential physics of ($S \cap B$) and ($S \cup B$) percolation.

The paper is organized as follows. In Section 2, the model is described and the finite size scaling analysis is discussed in Section 3. Details of the phase diagram obtained by finite size scaling analysis via Monte Carlo Simulations are shown in Section 3.1. The theoretical approach is introduced in Section 4 which includes the main results concerning the phase diagram obtained from the analytical calculations. Details of the calculations are given in the Appendix. The conclusions are drawn in Section 5.

2. The model

Let us consider a periodic triangular lattice of linear size L on which site monomers and bond monomers are independently deposited at random. The procedure is as follows: a site (bond) is randomly selected; if it is vacant, the site (bond) is then adsorbed on this site (bond). Otherwise, the attempt is rejected. In any case, the procedure is iterated until N_s sites and N_b bonds are adsorbed and the desired concentrations ($p_s = N_s/L^2$, $p_b = N_b/3L^2$) are reached. In the filling process, no overlap with previously added objects is allowed.

In order to calculate the percolation thresholds, one can think of a mapping $\mathbf{L} \to \mathbf{L}'$ from the original site–bond lattice $\mathbf{L}$ to an effective bond lattice $\mathbf{L}'$ where each bond and its endpoints sites of $\mathbf{L}$ transforms into an bond one of $\mathbf{L}'$. The rules for the mapping depend on the studied problem and the interested reader can be consult Ref. [22] for a detailed analysis of the study. Once the mapping is completed, each percolating (non-percolating) configuration in the effective lattice corresponds to a percolating (non-percolating) configuration in the original lattice. We use the standard Hoshen and Kopelman algorithm [23] for studying bond percolation on $\mathbf{L}'$. In the simulations performed in the paper the well-known Knuth random number generator has been used [24].

Every computational model is finite, and no singularities or discontinuities are ever observed in a finite system. The discontinuities and singularities which are of interest in the study of critical phenomena occur only in ideal infinite systems, and cannot be observed in any model which can be realized physically (and thus not in a computer model). The behavior of actual models is only an approximation to ideal behavior. The difficulty of using a finite lattice to simulate an infinite lattice can be eased somewhat by the use of so-called periodic boundary conditions. One wish is to embed the finite lattice in a virtual infinite lattice consisting of multiple copies of the finite lattice. All simulations in the paper are performed using periodic boundary conditions. Periodic boundary conditions can be applied in two ways for triangular lattices, i.e. twisted

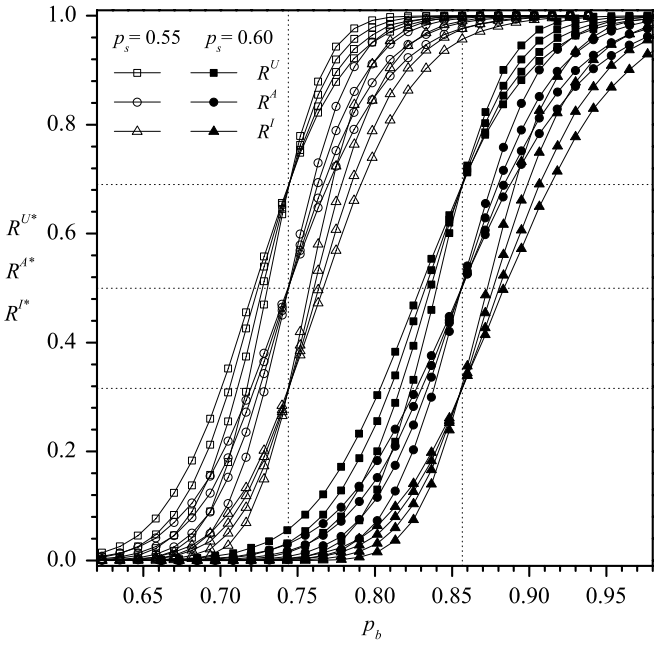

Fig. 1. Fraction of percolating lattices as a function of the concentration p_b. Different criteria, U (squares), I (triangles) and A (circles), are used for establishing the spanning cluster. Open symbols represent curves for $p_s = 0.55$ while filled symbols denote the case $p_s = 0.60$. Horizontal dashed lines show the R^{X*} universal points. Vertical dashed lines denote the percolation threshold in the thermodynamic limit $L \to \infty$. Different lattice sizes were used in the study ($L = 60, 72, 90, 120, 180, 240, 300$) but only $L = 60, 90, 180$ and 300 are shown in the figure for clarity.

(helical) boundary conditions and conventional boundary conditions. Conventional boundary conditions have been used throughout the paper without losing generality.

3. Finite-size scaling analysis

As the scaling theory predicts [5], the larger the system size to study, the more accurate the values of the threshold obtained therefrom. Thus, the finite-size scaling theory gives us the basis to achieve the percolation threshold and the critical exponents of a system with a desirable accuracy. For this purpose, the probability $R = R_L^X(p)$ that a lattice composed of $L \times L$ ($3L \times L$) sites (bonds) percolates at concentration p can be defined [2]. Here, as in Refs. [25,26], the following definitions can be given according to the meaning of X: (a) $R_L^I(p)$ = the probability of finding a cluster which percolates both in a rightward *and* in a downward direction; (b) $R_L^U(p)$ = the probability of finding either a rightward *or* a downward percolating cluster and (c) $R_L^A(p) \equiv \frac{1}{2}\left[R_L^I(p) + R_L^U(p)\right]$.

In the MC simulations, each MC run consists of the following steps: (a) the construction of the triangular lattice for the desired fractions p_s and p_b of site and bond, respectively; (b) the mapping from the original site–bond lattice to the effective bond lattice; and (c) the cluster analysis by using the Hoshen and Kopelman algorithm [23] on the effective bond lattice. In the last step, the existence of a percolating island is verified. This spanning cluster could be determined by using the criteria I, U and A. n runs of such two steps are carried out for obtaining the number m^X of them for which a percolating cluster of the desired criterion X is found. Then, $R_L^X(p_s, p_b) = m^X/n$ is defined and the procedure is repeated for different both values of (p_s, p_b) and lattice sizes. A set of $n = 5 \times 10^4$ independent samples are numerically prepared for each pair (p_s, p_b) and L ($L = 60, 72, 90, 120, 180, 240, 300$). From the point of view of calculations, we set p_s = constant and vary p_b.

In Fig. 1, the probabilities $R_L^I(p_b)$ (triangles), $R_L^U(p_b)$ (squares) and $R_L^A(p_b)$ (circles) are presented for $S \cap B$ percolation and two values of p_s (= 0.55 (empty symbols) and 0.60 (full symbols)). As it can be observed from Fig. 1, (a) for a given value of p_s, curves corresponding to different sizes cross each other in a unique universal point, R^{X*}, which depends on the criterion X used and (b) those points are located at very well defined values in the p_b-axes determining the critical percolation threshold for each p_s.

According to the theoretical prediction in Ref. [2], the critical exponent ν is determined from the divergence of the root mean square deviation of the threshold observed from their average values, Δ_L^X,

$$\Delta_L^X \propto L^{-1/\nu}. \tag{1}$$

As an example of the validity of the last equation, Fig. 2(a) (Fig. 3(a)) shows Δ_L^A as a function of L (note the log–log scale) for $p_s = 0.6$ ($p_s = 0.35$) for the case $S \cap B$ ($S \cup B$). According to Eq. (1), the slope of the line corresponds to $-1/\nu$, being $\nu = 1.324(8)$ ($\nu = 1.342(9)$) in this example.

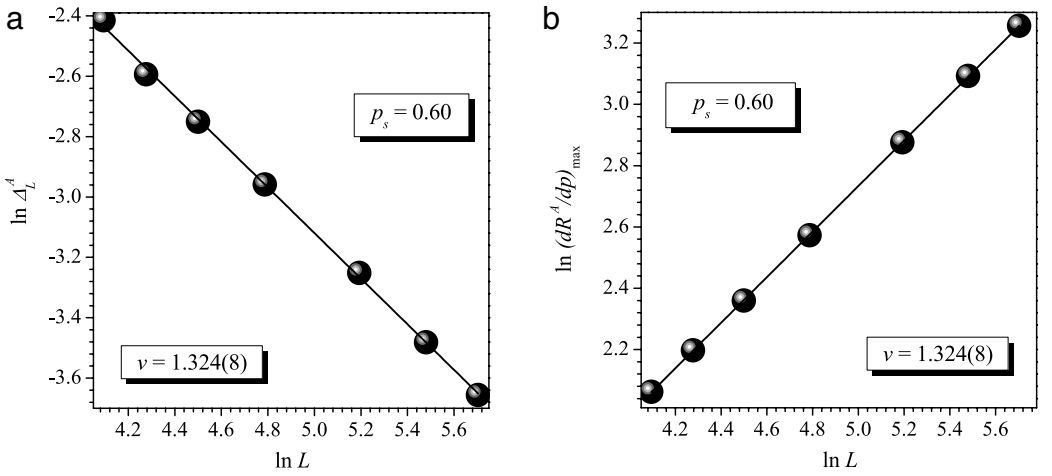

Fig. 2. (a) $\ln\left(\Delta_L^A\right)$ as a function of $\ln(L)$. According to Eq. (1) the slope corresponds to $-1/\nu$. (b) $\ln\left(\frac{dR^A}{dp_b}\right)_{\max}$ as a function of $\ln(L)$. The slope corresponds to $1/\nu$. Both cases correspond to $p_s = 0.60$.

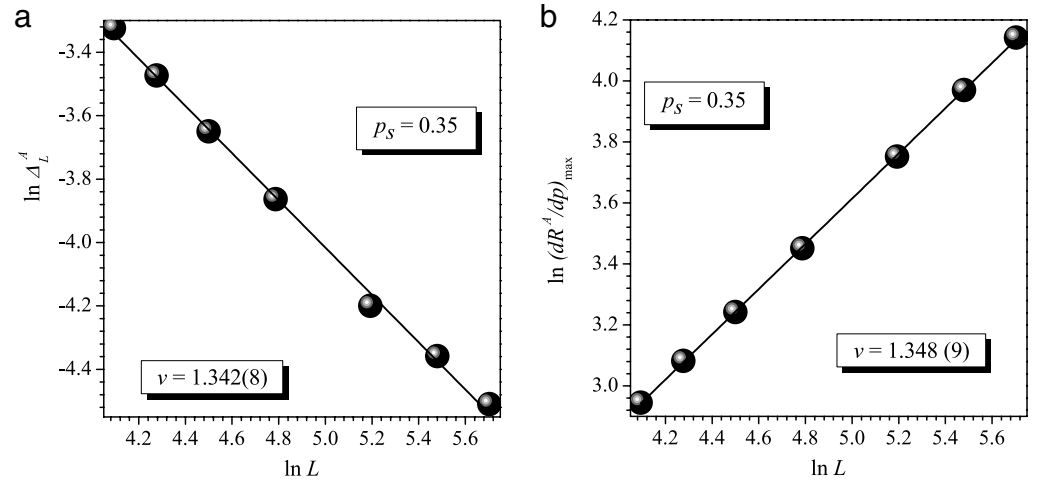

Fig. 3. (a) $\ln\left(\Delta_L^A\right)$ as a function of $\ln(L)$. According to Eq. (1) the slope corresponds to $-1/\nu$. (b) $\ln\left(\frac{dR^A}{dp_b}\right)_{\max}$ as a function of $\ln(L)$. The slope corresponds to $1/\nu$. Both cases correspond to $p_s = 0.35$.

Another alternative way for evaluating ν is given through the scaling relationship for R^X

$$R^X = \overline{R^X}\left[\left(p_b - p_b^c\right) L^{1/\nu}\right], \tag{2}$$

being $\overline{R^X}(u)$ the scaling function. Then, the maximum of the derivative of Eq. (2) leads to $\left(\frac{dR^X}{dp_b}\right)_{\max} \propto L^{1/\nu}$. In Fig. 2(b) (Fig. 3(b)) we have plotted $\left(\frac{dR^A}{dp_b}\right)_{\max}$ as a function of L (note the log–log scale) for different $p_s = 0.6$ ($p_s = 0.35$) for the case $S \cap B$ ($S \cup B$), whose slope corresponds to $1/\nu$. In this case, $\nu = 1.324(9)$ ($\nu = 1.348(9)$). By using both procedures for different values of p_s and the I, U, A criteria, it can be concluded that the results obtained for ν support the idea that the problem belongs to the same universality class as the random percolation on a square lattice as it was expected.

Once ν is known, Eqs. (2) allow for an efficient route to estimate p_b^c from the extrapolation of the positions $p_b^{cX}(L)$ of the maxima of the slopes of $R^X(L)$. For each criterion one expects that [2],

$$p_b^{cX}(L) = p_b^c + A^X L^{-1/\nu} \tag{3}$$

where A^X is a non-universal constant. Fig. 4(a) and (b) shows the extrapolation towards the thermodynamic limit of $p_b^{cX}(L)$ according to Eq. (3) for different criteria, for the case $p_s = 0.6$ ($S \cap B$) and $p_s = 0.35$ ($S \cup B$), respectively. These figures lend support to the assertion given by Eq. (3): (a) all the curves are well correlated by a linear function, (b) they have a quite similar value for the ordinate in the limit $L \to \infty$ and (c) the fitting determines a different value of the constant A

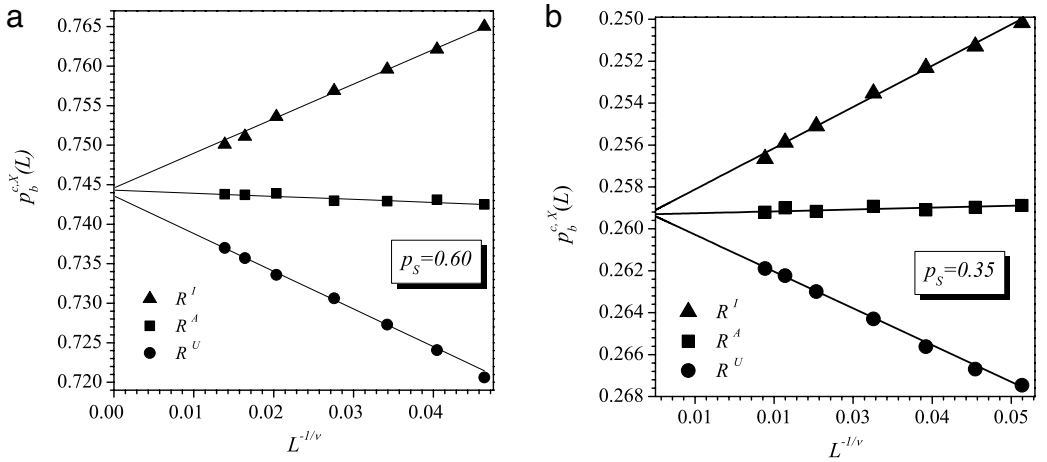

Fig. 4. Extrapolation of p_b^c towards the thermodynamic limit according to the theoretical prediction given by Eq. (3). Triangles, squares and circles denote the values of $p_b^c(L)$ obtained by using the criteria I, A and U, respectively. (a) $p_s = 0.60$ and (b) $p_s = 0.35$.

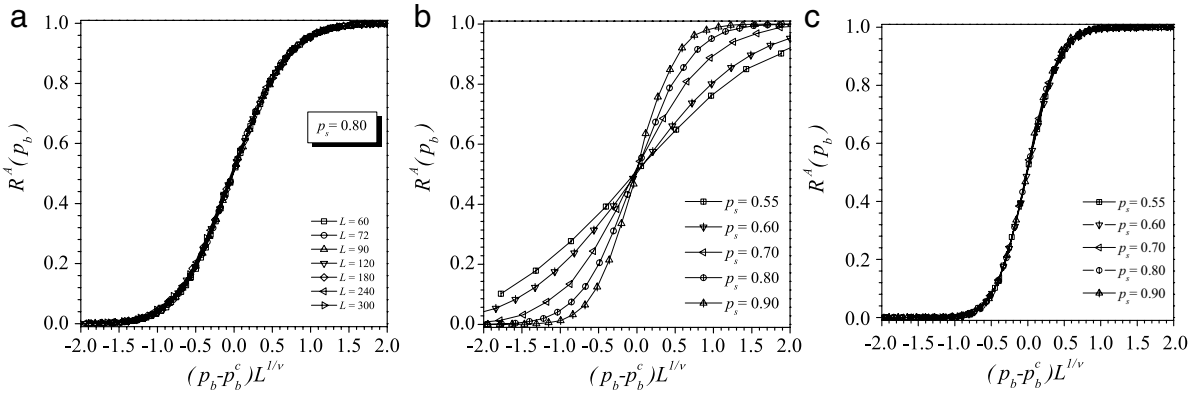

Fig. 5. (a) Collapsing plot of the curves for the fraction of percolating samples as a function of $u = \left(p_b - p_b^c\right) L^{1/\nu}$ for $p_s = 0.8$. Each symbol denotes a different value of L as indicated. (b) For each p_s, all the studied lattice sizes ($L = 60$, 72, 90, 120, 180, 240 and 300) collapse onto a universal curve. The solid lines are simply a visual guide. (c) The probability R^A as a function of the argument $u' = \left(p_b - p_b^c\right) L^{1/\nu} p_s^\theta$ where the metric factor p_s^θ is included in order to collapse all the curves in Fig. 5(b) onto a single one.

depending of the type of criterion used. It is also important to note that $p_b^{cA}(L)$ gives an almost perfect horizontal line which is a great advantage of the method because it does not require precise values of critical exponent ν in the process of estimating percolation thresholds. The maximum of the differences between $|p_b^{cI}(\infty) - p_b^{cA}(\infty)|$ and $|p_b^{cU}(\infty) - p_b^{cA}(\infty)|$ give the error bar for each determination of p_b^c.

The scaling law hypothesis also predicts the collapsing of the curves $R_L^X(p_b)$ when they are plotted as a function of a reduced variable $u = \left(p_b - p_b^c\right) L^{1/\nu}$, see Eq. (2). Thus, $\overline{R^X}$ is a universal function with respect to the variable u. In Fig. 5(a) this fact is shown for concentration $p_s = 0.8$ and different values of L as indicated. However, in Fig. 5(b), R^A is plotted as a function of u for each value of p_s as indicated (each value of p_s is represented by using a different symbol). Similar behavior can be obtained for U and I criteria. Two main conclusions can be drawn from the figure. Namely, (a) for a given value of p_s, all the curves used in the experiment (for different values of L) collapse into a universal curve according to the theoretical prediction. This gives an additional proof for the numerical value of the critical exponent ν. (b) $\overline{R^X}$ is not only a function of p_b and L but also of p_s. As it can be seen, the collapsing function is different for each value of p_s considered. This fact determines that the scaling function $\overline{R^X}$ is not a universal function with respect to the variable p_s.

In order to determine the dependence of $\overline{R^X}$ with p_s, the main features of the data shown in Fig. 5(b) have to be considered. As can be seen, the curves become steeper upon increasing the value of p_s. In fact, the derivative of the universal function $\overline{R^X}$ with respect to u becomes more pronounced as p_s increases. Then, it is possible to establish a power law to describe this behavior: $\left(\frac{\partial R^X}{\partial u}\right)_{\max} = B p_s^\lambda$. On the other hand, the derivatives are narrowed upon increasing p_s. This behavior can also be described by a power law according to $\Delta^X = C p_s^{-\theta}$, being Δ^X the root mean square deviation of $\left(\frac{\partial R^X}{\partial u}\right)$ for each curve.

Table 1
Numerical values of (p_b, p_s) for de case percolation $S \cap B$. Error estimates concerning the last digit(s) are indicated between brackets.

p_b	p_s
0.3560(4)	0.998
0.3599(5)	0.975
0.3735(5)	0.950
0.4031(4)	0.9
0.4370(4)	0.85
0.4781(3)	0.8
0.5256(4)	0.75
0.5843(5)	0.7
0.6534(5)	0.65
0.7439(4)	0.6
0.8566(3)	0.55
1.0000	0.500(3)

Table 2
Numerical values of (p_b, p_s) for de case percolation $S \cup B$. Error estimates concerning the last digit(s) are indicated between brackets.

p_b	p_s
0.0000	0.500(3)
0.1281(5)	0.475
0.1705(5)	0.45
0.2233(4)	0.4
0.2597(3)	0.35
0.2861(4)	0.3
0.3217(6)	0.2
0.3417(5)	0.1
0.3470(4)	0.0

The maxima of the derivatives (the standard deviation of each derivative) for each value of p_s as a function of p_s can be plotted in a log–log scale (not shown here). The points are very well correlated by a linear function with the fitting parameters $\lambda = 2.03(2)$ and $\theta = 2.3(2)$. The number between parentheses is the error in the determination of the corresponding informed quantities.

According to the equations above, a metric factor might to be included in the scaling function, Eq. (2), in order to collapse all the curves in Fig. 5(b) onto a single one. Following Ref. [27], in Fig. 5(c) we plot the probability R^X as a function of the argument $u' = \left(p_b - p_b^c\right) L^{1/\nu} p_s^{\theta}$. As clearly observed, all the curves in Fig. 5(b) collapse onto a single one. It is remarkable that more than 3×10^3 points are included in the collapsing curve. The metric factor introduced here, p_s^{θ}, gives an additional proof for the numerical value of the exponent θ obtained from the behavior of $\Delta^X(p_s)$. A completely similar procedure can be conducted whether p_b is kept fixed while p_s is varied in the whole range.

3.1. Phase diagram

The finite-size scaling analysis has been used in the whole range of the variables p_s and p_b in order to determine the percolation thresholds and the phase diagram in the case of monomers deposited on a triangular lattice. Thus, the resulting $p_s - p_b$ phase diagram for site–bond percolation (solid symbols) is shown in Fig. 6 (circles for $S \cap B$ and stars for $S \cup B$). These numerical results are shown in Tables 1 and 2. In Fig. 6 our results are compared with previous ones of Ref. [16], shown as small triangles. There is an excellent agreement with previous results in the literature.

The main characteristics of the phase diagram are: (1) the critical curve corresponding to the $S \cap B$ model varies between the point $[p_s = 1.0, p_b = 0.3473(2)]$ on the left and the point $[p_s = 0.500(2), p_b = 1.0]$ on the right, where $p_b = 0.3473(2)$ and $p_s = 0.500(2)$ are the percolation thresholds for bond and site percolation on a triangular lattice, respectively and (2) the critical curve corresponding to the $S \cup B$ model varies between the point $[p_s^c = 0.500(2), p_b = 0.0]$ on the left and the point $[p_s = 0.0, p_b = 0.3473(2)]$ on the right.

First, we shall compare our Monte Carlo results with the approximate formula proposed in Refs. [15,16]. In fact, Hammersley [1] proved for a partially directed graph a theorem which yields the inequality

$$P(p_s p_b, 1) \leq P(p_s, p_b) \leq P(1, p_s p_b), \tag{4}$$

where $P(p_s, p_b)$ is the percolation probability (i.e. the probability that a single source site is connected to an infinite set of other sites). The inequality Eq. (4) gives reasonably sharp bounds for the mixed percolation probability. For a Bethe lattice ($p_{cb} = p_{cs} = p_c$, where p_{cs} is the threshold for pure site percolation, and p_{cb} is the one for pure bond percolation) we can get

$$p_s p_b = p_c. \tag{5}$$

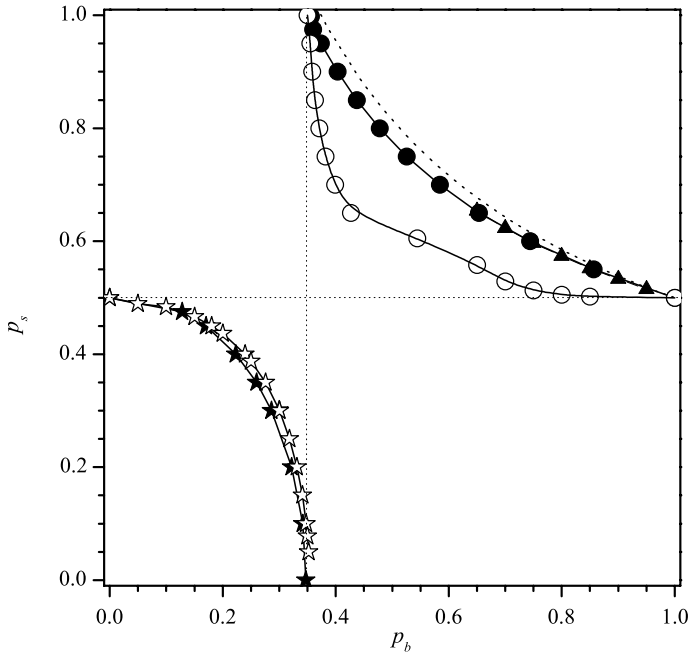

Fig. 6. Phase diagram of site–bond percolation for a triangular lattice obtained by finite-size scaling simulations (solid circles for $S \cap B$ and solid stars for $S \cup B$) and the same phase diagram obtained from the theoretical approach (empty circles for $S \cap B$ and empty stars for $S \cup B$). Triangles are results from Ref. [16] and the dashed line denotes Eq. (6).

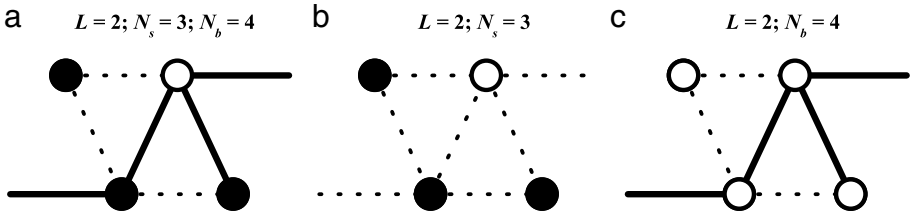

Fig. 7. (a) Snapshot corresponding to a 2×2 cell with three occupied sites ($N_s = 3$) and four occupied bonds ($N_b = 4$). Solid circles, open circles, solid lines and dotted lines represent occupied sites, empty sites, occupied bonds and empty bonds, respectively. (b) Site lattice corresponding to the configuration shown in part (a). (c) Bond lattice corresponding to the configuration shown in part (a).

The shape of the boundary between percolation and non-percolation was subsequently studied by Yanuka and Englman [15]. They proposed the following equation for the critical curve in the (p_b, p_s) plane:

$$\frac{\log p_s}{\log p_{cs}} + \frac{\log p_b}{\log p_{cb}} = 1. \tag{6}$$

The equation satisfies the inequality Eq. (4) and gives the correct limit Eq. (5) for a Bethe lattice. The equation defines a line in the (p_b, p_s) plane, starting at $(p_{cb}, 1)$ and ending at $(1, p_{cs})$, as is shown as a dashed line in Fig. 6. Monte Carlo simulation results lie remarkably close to the line defined by Eq. (6).

4. The theoretical approach: phase diagram

The theoretical approach is based on exact calculations of configurations [28,29] with the following assumptions: (i) the original problem is divided into separated site and bond problems that are independently analyzed (see Fig. 7); (ii) the percolation is measured along the x-axis; and (iii) symmetric $L \times L$ cells are used in the calculations. The percolation trajectory ℓ is defined as the number of objects belonging to the percolating cluster. Thus, the minimum percolation trajectory, represented by $\ell_{\min}$, corresponds to the direct percolation path from left to right (or vice versa), being $\ell_{\min} = L$ for sites and bonds. On the other hand, the maximum percolation trajectory, represented by $\ell_{\max}$, corresponds to the number of objects in the saturated cell, being $\ell_{\max} = L^2$ and $3L(L-1)+1$ for sites and bonds, respectively (see Fig. 7). In general, the length of a percolation trajectory varies between $\ell_{\min}$ and $\ell_{\max}$.

In the case of sites, the probability of percolation for any given cell considers the addition of the individual probabilities of all percolating trajectories leading to a polynomial function $f(p_s)$, where $\ell_{\min} = L$ determines the minimum degree of the

polynomial function, and $\ell_{\max} = L^2$ corresponds to the maximum degree associated to it. Then,

$$f(p_s) = \sum_{\ell=\ell_{\min}}^{\ell_{\max}} C_\ell^s p_s^\ell (1-p_s)^{\ell_{\max}-\ell}, \tag{7}$$

where the coefficients C_ℓ^s's correspond to the totality of the site trajectories of length ℓ leading to percolation. For a 2×2 cell, Eq. (7) results

$$f(p_s) = 3p_s^2 - 2p_s^3. \tag{8}$$

In the case of bonds, the corresponding polynomial function $g(p_b)$ can be written as

$$g(p_b) = \sum_{\ell=\ell_{\min}}^{\ell_{\max}} C_\ell^b p_b^\ell (1-p_b)^{\ell_{\max}-\ell}, \tag{9}$$

where $\ell_{\min} = L$, $\ell_{\max} = 3L(L-1)+1$ and C_ℓ^b's correspond to the totality of the bond trajectories of length ℓ leading to percolation. For a 2×2 cell, Eq. (10) results

$$g(p_b) = 4p_b^2 + 3p_b^3 - 20p_b^4 + 23p_b^5 - 11p_b^6 + 2p_b^7. \tag{10}$$

Once $f(p_s)$ and $g(p_b)$ are obtained, the percolation functions corresponding to $S \cap B$ and $S \cup B$ site–bond percolation are calculated by following the Tsallis scheme [30],

$$h_{S\cap B}(p_s, p_b) = f(p_s)g(p_b) \tag{11}$$

and

$$h_{S\cup B}(p_s, p_b) = f(p_s) + g(p_b) - f(p_s)g(p_b). \tag{12}$$

Then, for a 2×2 cell,

$$h_{S\cap B}(p_s, p_b) = (3p_s^2 - 2p_s^3)(4p_b^2 + 3p_b^3 - 20p_b^4 + 23p_b^5 - 11p_b^6 + 2p_b^7) \tag{13}$$

and

$$\begin{aligned} h_{S\cup B}(p_s, p_b) = {} & (3p_s^2 - 2p_s^3) + (4p_b^2 + 3p_b^3 - 20p_b^4 + 23p_b^5 - 11p_b^6 + 2p_b^7) \\ & - (3p_s^2 - 2p_s^3)(4p_b^2 + 3p_b^3 - 20p_b^4 + 23p_b^5 - 11p_b^6 + 2p_b^7). \end{aligned} \tag{14}$$

$h_{S\cap B}(p_s, p_b)$ (Eq. (13)) and $h_{S\cup B}(p_s, p_b)$ (Eq. (14)) are plotted in Fig. 8(a) and (b), respectively. These curves are necessary in order to obtain the curves delimiting the phases (the percolating and non-percolating areas) present in the problem. Accordingly, the $p_s - p_b$ phase diagram can be obtained by the procedure described in the Appendix and the results are shown in Fig. 6 (open symbols, circles for $S \cap B$ and stars for $S \cup B$). As can be observed, a very good qualitative agreement is obtained between simulation and analytical data. From a quantitative point of view, the theoretical results for $S \cap B$ and $S \cup B$ differ by 11.12% and 3.71%, respectively, from the simulation values.[1]

5. Conclusions

In this work, the phase diagram of the site–bond percolation problem for triangular lattices has been addressed. By using extensively Monte Carlo simulations and finite-size scaling analysis the phase diagram of the $S \cup B$ and the $S \cap B$ model were determined.

In order to test the universality of the problem, the phase transition involved on it has been studied by using finite-size scaling theory. In particular, it was established that (a) if p_b (p_s) remains constant the scaling functions are dependent with respect to the coordinate p_s (p_b) and (b) the problem, in all the studied cases, belongs to the random percolation universality class. The last conclusion can be also confirmed by determining the numerical values of the critical exponents, and the fractal dimension of the spanning cluster.

Monte Carlo results were compared with theoretical data. For this purpose, the site–bond percolation problem on triangular lattices has been studied by using a theoretical approach, which is based on exact calculation of configurations on finite cells. From the counting of the number of configurations leading to percolation, the $S \cup B$ and $S \cap B$ percolating functions were introduced. Taking advantage of their definitions, the $p_s - p_b$ phase diagram was calculated. A very good qualitative agreement was obtained between simulation and analytical data. From a quantitative point of view, the theoretical results for $S \cap B$ and $S \cup B$ differ by 11.12% and 3.71%, respectively, from the simulation values. The theoretical approach used throughout the paper has shown to be effective when it was used for the study of two-dimensional square lattices:

[1] The value 11.12% (3.71%) has been calculated from the difference between theoretical and simulation $S \cap B$ ($S \cup B$) areas.

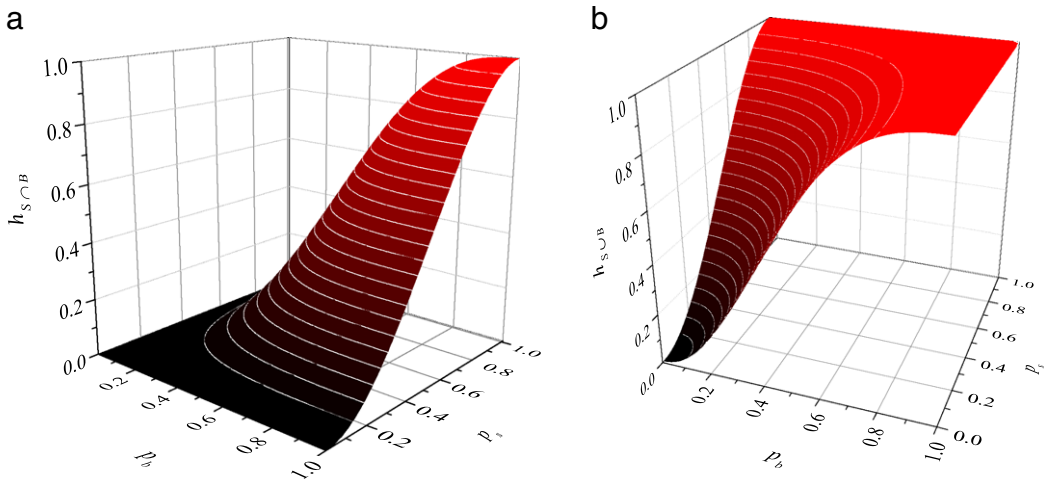

Fig. 8. (a) Percolation function $h_{S\cap B}(p_s, p_b)$ (Eq. (13)) as a function of p_s and p_b. (b) Same as part (a) for $h_{S\cup B}(p_s, p_b)$ (Eq. (14)).

(a) monomers [28,31,32] and (b) dimers [29] *and* for three dimensional cubic lattices [33]. The method has shown to be effective in order to determine the critical percolation threshold as well as the critical exponents of the phase transition involved in the problem. The results presented here are comparable with those reported for the same problem for square lattices.

Finally, the present study encourages us to determine the phase diagram of the site–bond percolation when the size of the percolating species is increased. This work is in progress.

Acknowledgments

W.L. is thankful for support from Universidad de la Frontera (Temuco, Chile) under project DIDUFRO, DI13-0102. M.G., P.C., F.N. and A.J.R.P. thank support from Universidad Nacional de San Luis (Argentina) under project 322000, CONICET (Argentina) under project PIP 112-201101-00615 and the National Agency of Scientific and Technological Promotion (Argentina) under project PICT-2010-1466. Partial support from FONDECYT (Chile) under project 1100156, Millennium Scientific Nucleus "Basic and Applied Magnetism" and Center for the Development of Nanoscience and Nanotechnology is also acknowledged.

Appendix

Once the functions $h_{S\cap B}(p_s, p_b)$ (Eq. (13)) and $h_{S\cup B}(p_s, p_b)$ (Eq. (14)) are determined, the projections of these surfaces on the planes (p_b = constant) and (p_s = constant) behave in a similar way to the curves of the percolation order parameter obtained with respect to one variable while keeping the second constant. Accordingly, the mentioned projections show a change in the concavity (inflection points), which can be associated to the existence of a transition from a non-percolating to a percolating state.

A way to study the local curvature of $h_{S\cap B}(p_s, p_b)$ and $h_{S\cup B}(p_s, p_b)$ is by using the concept of gradient. Thus,

$$\begin{aligned}\vec{\nabla} h_{S\cap B}(p_s,p_b) &= \frac{\partial h_{S\cap B}(p_s,p_b)}{\partial p_s}\widehat{p_s} + \frac{\partial h_{S\cap B}(p_s,p_b)}{\partial p_b}\widehat{p_b} \\ &= \left[g(p_b)\frac{\partial f(p_s)}{\partial p_s}\right]\widehat{p_s} + \left[f(p_s)\frac{\partial g(p_b)}{\partial p_b}\right]\widehat{p_b}; \end{aligned} \tag{15}$$

and

$$\begin{aligned}\vec{\nabla} h_{S\cup B}(p_s,p_b) &= \frac{\partial h_{S\cup B}(p_s,p_b)}{\partial p_s}\widehat{p_s} + \frac{\partial h_{S\cup B}(p_s,p_b)}{\partial p_b}\widehat{p_b} \\ &= \left[\frac{\partial f(p_s)}{\partial p_s} - g(p_b)\frac{\partial f(p_s)}{\partial p_s}\right]\widehat{p_s} + \left[\frac{\partial g(p_b)}{\partial p_b} - f(p_s)\frac{\partial g(p_b)}{\partial p_b}\right]\widehat{p_b}. \end{aligned} \tag{16}$$

Now, the modulus of the gradients $\left\|\vec{\nabla} h_{S\cap B}(p_s,p_b)\right\|$ and $\left\|\vec{\nabla} h_{S\cup B}(p_s,p_b)\right\|$ can be calculated as:

$$S_{S\cap B} = \left\|\vec{\nabla} h_{S\cap B}(p_s,p_b)\right\| = \sqrt{\left[g(p_b)\frac{\partial f(p_s)}{\partial p_s}\right]^2 + \left[f(p_s)\frac{\partial g(p_b)}{\partial p_b}\right]^2}; \tag{17}$$

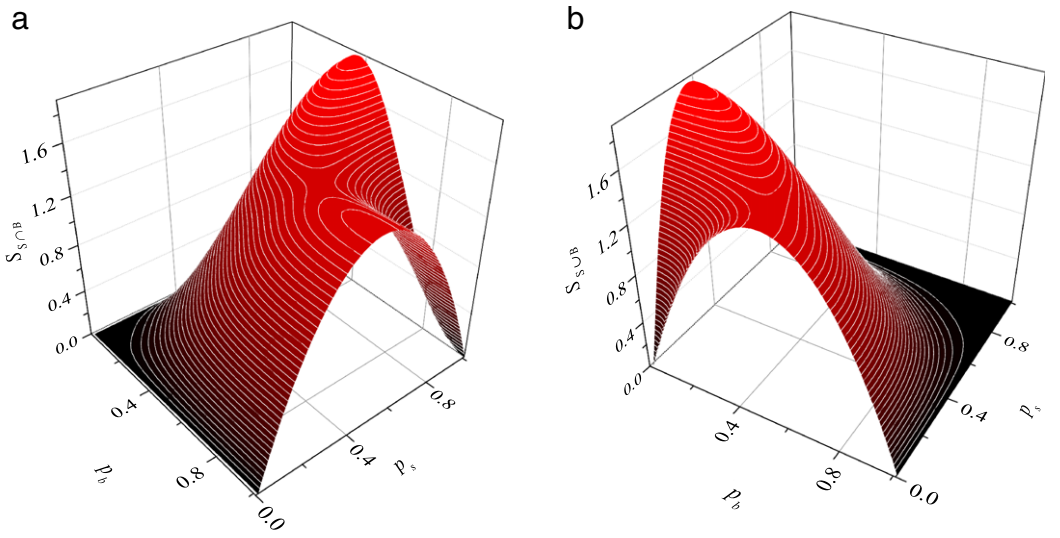

Fig. 9. (a) $S_{S\cap B}$ and (b) $S_{S\cup B}$ which are given by Eqs. (17) and (18) as a function of p_s and p_b.

and

$$S_{S\cup B} = \left\| \vec{\nabla} h_{S\cup B}(p_s, p_b) \right\| = \sqrt{\left[\frac{\partial f(p_s)}{\partial p_s} - g(p_b) \frac{\partial f(p_s)}{\partial p_s} \right]^2 + \left[\frac{\partial g(p_b)}{\partial p_b} - f(p_s) \frac{\partial g(p_b)}{\partial p_b} \right]^2}. \tag{18}$$

$S_{S\cap B}$ and $S_{S\cup B}$ are shown in Fig. 9(a) and (b), respectively. As it can be observed, the curves for a fixed value of p_b present a maximum for a given value of p_s, and in the same manner, the curves for a fixed value of p_s present a maximum for a given value of p_b. The set of such maxima can be calculated in the following way (for simplicity we restrict to the $S \cap B$ case, the methodology used for the $S \cup B$ case is identical):

(1) Setting $\partial S_{S\cap B}/\partial p_s$ (for different fixed values of p_b) equal to zero, a set of points $(p_s, p_b)_1$ is obtained.
(2) Setting $\partial S_{S\cap B}/\partial p_b$ (for different fixed values of p_s) equal to zero, a set of points $(p_s, p_b)_2$ is obtained.

The common points obtained from (1) and (2) determine two critical points, ($p_s = 0.5, p_b = 1.0$) and ($p_s = 1.0, p_b = 0.3536$), which correspond to the limits of the $S \cap B$ curve in Fig. 6. We propose to calculate the intermediate points of the $S \cap B$ curve from the sets $(p_s, p_b)_1$ and $(p_s, p_b)_2$ and the use of the Hessian criterion to determine the nature of the critical points. For this purpose, the Hessian matrix is built as

$$H = \begin{pmatrix} \dfrac{\partial^2 S_{S\cap B}}{\partial p_s^2} & \dfrac{\partial^2 S_{S\cap B}}{\partial p_s \partial p_b} \\ \dfrac{\partial^2 S_{S\cap B}}{\partial p_b \partial p_s} & \dfrac{\partial^2 S_{S\cap B}}{\partial p_b^2} \end{pmatrix}. \tag{19}$$

Then, the $S \cap B$ critical curve is obtained by collecting the points that (i) belong to the sets $(p_s, p_b)_1$ and $(p_s, p_b)_2$ and (ii) satisfy the local maximum conditions ($|H| > 0$ and $\frac{\partial^2 S}{\partial p_s^2} < 0$). The same procedure is used for the $S \cup B$ case. The resulting critical points are shown as empty symbols in the phase diagram shown in Fig. 6.

References

[1] J.M. Hammersley, Proc. Cambridge Philos. Soc. 53 (1957) 642.
[2] D. Stauffer, Introduction to Percolation Theory, Taylor & Francis, 1985.
[3] R. Zallen, The Physics of Amorphous Solids, John Willey & Sons, NY, 1983.
[4] J.W. Essam, Rep. Progr. Phys. 43 (1980) 833.
[5] K. Binder, Rep. Progr. Phys. 60 (1997) 488.
[6] C. Lorenz, R. May, R. Ziff, J. Stat. Phys. 98 (2000) 961.
[7] M. Aizenman, Nucl. Phys. B 485 (1997) 551.
[8] J. Cardy, J. Phys. A 31 (1998) L105–L110.
[9] L.N. Shchur, S.S. Kosyakov, Internat. J. Modern Phys. C 8 (1997) 473.
[10] L.N. Shchur, in: D.P. Landau, S.P. Lewis, H.B. Schuettler (Eds.), Incipient Spanning Clusters in Square and Cubic Percolation, in: Springer Proceedings in Physics, vol. 85, Springer-Verlag, Heidelberg, Berlin, 2000.
[11] A. Coniglio, H.E. Stanley, W. Klein, Phys. Rev. Lett. 42 (1979) 518.
[12] H.L. Frisch, J.M. Hammersley, J. Soc. Ind. Appl. Math. 11 (1963) 894.
[13] P. Agrawal, S. Render, P.J. Reynolds, H.E. Stanley, J. Phys. A: Math. Gen. 12 (1979) 2073.

[14] H. Nakanishi, J. Reynolds, Phys. Lett. A 71 (1979) 252.
[15] M. Yanuka, R. Englman, J. Phys. A: Math. Gen. 23 (1990) L339.
[16] Y.Y. Tarasevich, S.C. van der Marck, Internat. J. Modern Phys. C 10 (1999) 1193.
[17] F.Y. Wu, Phys. Rev. E 81 (2010) 06110.
[18] C. Ding, Z. Fu, W. Guo, F.Y. Wu, Phys. Rev. E 81 (2010) 061111.
[19] F.Y. Wu, J. Phys. A: Math. Gen. 14 (1981) L39.
[20] I.G. Enting, F.Y. Wu, J. Stat. Phys. 28 (1982) 351.
[21] R.L. Holtz, J. Phys. A: Math. Gen. 21 (1988) 1303.
[22] M. Dolz, F. Nieto, A.J. Ramirez-Pastor, Eur. Phys. J. B 43 (2005) 363.
[23] J. Hoshen, R. Kopelman, Phys. Rev. B 14 (1976) 3438;
J. Hoshen, R. Kopelman, E.M. Monberg, J. Stat. Phys. 19 (1978) 219.
[24] D.E. Knuth, The Art of Computer Programming, Vol. 2: Seminumerical Algorithms, second ed., Addison-Wesley, Reading, MA, 1981.
[25] F. Yonezawa, S. Sakamoto, M. Hori, Phys. Rev. B 40 (1989) 636.
[26] F. Yonezawa, S. Sakamoto, M. Hori, Phys. Rev. B 40 (1989) 650.
[27] V. Privman, P.C. Hohenberg, A. Aharony, in: C. Domb, J.L. Lebowitz (Eds.), Universal Critical-Point Amplitude Relations, in: Phase Transitions and Critical Phenomena, vol. 14, Academic, NY, 1991, pp. 1–134. 364–367 (Chapter 1).
[28] E.E. Vogel, W. Lebrecht, J.F. Valdés, Physica A 389 (2010) 1512.
[29] W. Lebrecht, J.F. Valdés, E.E. Vogel, F. Nieto, A.J. Ramirez-Pastor, Physica A 392 (2013) 149.
[30] C. Tsallis, Physica A 344 (2004) 718.
[31] W. Lebretch, J.F. Valdes, Rev. Mexicana Fís. 54 (2008) 349.
[32] W. Lebretch, Rev. Mexicana Fís. 56 (2010) 190.
[33] W. Lebretch, M.I. Gonzalez, Rev. Mexicana Fís. 57 (2011) 344.